Mon. Not. R. Astron. Soc. **000**, 1–13 (2016) Printed 12 January 2017 (MN LATEX style file v2.2)

The dynamics of the local group as a probe of Dark Energy and Modified Gravity

Edoardo Carlesi [1], David F. Mota [2], Hans A. Winther [3,4]
⋆ [1] *Racah Institute of Physics, Givat Ram, 91040 Jerusalem, Israel*
[2] *Institute for Theoretical Astrophysics, University of Oslo, Norway*
[3] *Astrophysics, University of Oxford, DWB, Keble Road, Oxford, OX1 3RH, United Kingdom*
[4] *Institute of Cosmology and Gravitation, University of Portsmouth,Burnaby Road, Portsmouth PO1 3FX, United Kingdom*

Submitted XXXX XXX XXXX

ABSTRACT
In this work we study the dynamics of the Local Group (LG) within the context of cosmological models beyond General Relativity (GR). Using observable kinematic quantities to identify candidate pairs we build up samples of simulated LG-like objects drawing from $f(R)$, symmetron, DGP and quintessence *N*-body simulations together with their ΛCDM counterparts featuring the same initial random phase realisations. The variables and intervals used to define LG-like objects are referred to as Local Group model; different models are used throughout this work and adapted to study their dynamical and kinematic properties. The aim is to determine how well the observed LG-dynamics can be reproduced within cosmological theories beyond GR, We compute kinematic properties of samples drawn from alternative theories and ΛCDM and compare them to actual observations of the LG mass, velocity and position. As a consequence of the additional pull, pairwise tangential and radial velocities are enhanced in modified gravity and coupled dark energy with respect to ΛCDM inducing significant changes to the total angular momentum and energy of the LG. For example, in models such as $f(R)$ and the symmetron this increase can be as large as 60%, peaking well outside of the 95% confidence region allowed by the data. This shows how simple considerations about the LG dynamics can lead to clear small-scale observational signatures for alternative scenarios, without the need of expensive high-resolution simulations.

Key words: Cosmology, Numerical simulations, Dark matter, Local Group

1 INTRODUCTION

The accelerated expansion of the Universe still remains largely unexplained since its discovery at the turn of the century (Riess et al. 1998; Perlmutter et al. 1999). One way to account for it is adding an extra component with negative equation of state to the General Relativity (GR) Lagrangian, the so called dark energy (DE). In its simplest form, DE takes the form of a cosmological constant (Λ) which together with the Cold Dark Matter (CDM) paradigm defines the current standard concordance model ΛCDM. Despite its simplicity and its successes, a number of theoretical problems (see Bull et al. 2016, for a comprehensive review) have led the theorists to devise models of dynamical dark energy, with a time-dependent equation of state, such as quintessence (Wetterich 1995; Caldwell et al. 1998; Copeland et al. 1998; Zlatev et al. 1999), vector dark energy (Beltrán Jiménez & Maroto 2008; Carlesi et al. 2012), $\kappa-$essence (Armendariz-Picon et al. 2000) and Chaplygin gas (Kamenshchik et al. 2001) to mention some among the great number of models elaborated during the last years.

However, DE (in both its static and dynamic form) is not the only possible explanation for the late time acceleration of the Universe: an alternative mechanism for this involves large scales modifications of GR (see Clifton et al. 2012, for a comprehensive review). This latter class of theories usually introduces an additional scalar degree of freedom alongside the usual massless spin-2 graviton of GR, which effectively acts as a fifth force. In general, in order to keep this class of theories consistent with local GR tests (Will 2014), it is necessary to introduce some kind of interaction-screening within high-density regions (Khoury 2010).

Cosmological simulations of dark energy models (Baldi 2012) and modified gravity (Winther et al. 2015) have emerged over the last decade as the main tool to study several aspects of the non-linear regime of theories beyond ΛCDM. For instance, they have been used to look for signatures in the matter power spectrum and mass functions (Macciò et al. 2004; Baldi et al. 2010; Cui et al. 2012; Viel et al. 2012; Li et al. 2012; Puchwein et al. 2013; Mota et al. 2007; He et al. 2015; Mota et al. 2008; Vargas dos Santos et al. 2016), in voids, environment and the cosmic web (Li & Barrow 2011; Winther et al. 2012; Shim et al. 2014; Falck et al.

⋆ E-mail: carlesi@phys.huji.ac.il

2014; Carlesi et al. 2014a; Elyiv et al. 2015; Sutter et al. 2015; Pollina et al. 2016), and in the properties of galaxy clusters (Lee & Baldi 2012; Llinares & Mota 2013; Carlesi et al. 2014b; Hammami et al. 2015; Gronke et al. 2015; Arnold et al. 2014).

Model selection among the great number of alternatives to the standard paradigm, devising new tests that might help constrain their free parameters and their consistency, is a fundamental task of theoretical cosmology. In this work we introduce a new way of estimating the viability of several types of modified gravity and dark energy models, which employs *N*-body simulations and uses the observed dynamics of the Local Group (LG) of galaxies as a cosmological probe. We focus on the properties of its two most prominent members, the Milky Way (MW) and Andromeda (M31) spirals, to determine whether alternative theories can account for their observed kinematics. This is a computationally cheap and conceptually simple way of using astrophysical scales, cosmology-independent data as a test for theories beyond GR. In fact, since in such an approach halos are treated as point-like particles, disregarding the details of inner structure, one does not have to rely on expensive high-resolution simulations to deal with the sub-megaparsec regime of alternative cosmologies.

We focus here on several models where a fifth-force kind of interaction is introduced: coupled quintessence (Amendola 2000), $f(R)$ (Hu & Sawicki 2007), the symmetron (Hinterbichler & Khoury 2010) and DGP (Dvali et al. 2000). In these cases, deviations from standard Newtonian gravity and the enhancement of particles' accelerations (a common feature of most fifth-force models, see e.g. Baldi et al. 2010; Gronke et al. 2015; Shi et al. 2015) is expected to affect the two body dynamics of the LG in a systematic way, providing clear observational signatures (Hellwing et al. 2014). The aim of the present work is to quantify these signatures and compare them to the observations, in order to determine which models (or parameters) turn out to be at odds (or in agreement) with the known LG dynamics. This is achieved by computing posterior distribution functions (PDF) for a series of dynamic (energy and momentum) and kinematic (radial and tangential velocity components) variables, using samples of LG-like objects found in the simulations. To reduce the arbitrariness in the definition of a *simulated* Local Group, we employ several definitions using different observationally-motivated parameters and intervals, which we refer to as *models* of the LG. The PDFs are then computed for each LG model and each simulation. Comparing these functions to the actual values, we can establish to which extent a cosmology is expected to account for the observed LG dynamics.

Of course, one may ask about the statistical relevance of such a procedure given that we have data related to only *one* LG. Doing cosmology with a single object however is not a new challenge, and despite its limitations, it has been successfully employed e.g. in the case of massive high-z galaxy clusters (Baldi & Pettorino 2011; Carlesi et al. 2011; Harrison & Coles 2011; Waizmann et al. 2011) and the bullet cluster (Lee & Baldi 2012), where single, peculiar objects have been used to evaluate whether their existence could be considered a normal outcome of the model or else was indicating some inconsistency. Moreover, the idea is in line with the concept of *near-field cosmology* (Bland-Hawthorn & Peebles 2006), that aims to extract cosmologically relevant informations from the study of nearby objects, under the assumption that our patch of the Universe is not an extraordinary environment but rather a common kind of place. This assertion could be of course contradicted invoking some kind of anthropic principle, arguing that our galaxy is an outlier and a one-of-a-kind object inside our Universe. Rejecting the latter hypothesis, however, it becomes meaningful to analyse the properties of MW size objects for cosmological purposes, as it has been done in recent years to argue against ΛCDM (Kroupa et al. 2012; Pawlowski et al. 2015), in favour of it (Libeskind et al. 2015), or to compare it to alternative models (Penzo et al. 2014; Elahi et al. 2015; Macciò et al. 2015; Penzo et al. 2016).

This paper is structured as follows. Section 2 briefly introduces the main motivations, mathematical and physical features that characterize the different class of models (quintessence, symmetron and $f(R)$) that will be discussed later. Section 3 contains a description of the simulations, the parameters used and the basic properties of the non-standard *N*-body codes used. In Section 4 we discuss the main ideas behind our formalism and the properties of the observational data it relies upon. The results of our analysis are then presented in Section 5, where we discuss the implications for the viability and non viability of some of the models presented here. A summary of the techniques and the results discussed throughout the *Paper* is presented in Section 6.

2 MODELS

This section provides a short introduction to the main physical and mathematical properties of the models discussed. References to more accurate descriptions are provided in each subsection for the interested reader.

2.1 DGP

DGP (Dvali et al. 2000) is a so-called braneworld model where matter lives on a 4D brane which is embedded in a 5D spacetime. The action is given by

$$S = \int \sqrt{-g_{(4)}}\mathrm{d}^4x \frac{M^2_{\mathrm{Pl}\,(4)}}{2} R_{(4)} + \int \sqrt{-g_{(5)}}\mathrm{d}^5x \frac{M^2_{\mathrm{Pl}\,(5)}}{2} R_{(5)} \tag{1}$$

where $g_{(4)}$ denotes the induced 4D metric on the brane, $R_{(4)}$ the induced Ricci scalar on the brane, $g_{(5)}$ the metric in the bulk and $R_{(5)}$ the Ricci scalar in the bulk.

The ratio of the two Planck masses, $r_c = \frac{1}{2}\left(\frac{M_{\mathrm{Pl}\,(4)}}{M_{\mathrm{Pl}\,(5)}}\right)^2$, is the only free parameter of the model known as the crossover scale. For scales $r \ll r_c$ gravity behaves as being four dimensional while for $r \gtrsim r_c$ the five dimensional aspects become important.

The modifications to gravitational force is determined by a scalar field ϕ called the brane-bending mode. The brane-bending mode influences the dynamics of particles through a gravitational potential

$$\Phi = \Phi_N + \frac{\phi}{2} \tag{2}$$

where Φ_N is the standard Newtonian potential, i.e. $\nabla^2\Phi_N = 4\pi G a^2 \delta\rho_m$. The dynamics of ϕ in the quasi-static approximation (Winther & Ferreira 2015) is given by

$$\nabla^2\phi + \frac{r_c^2}{3\beta a^2}\left[(\nabla^2\phi)^2 - (\nabla_i\nabla_j\phi)^2\right] = \frac{a^2\delta\rho}{\beta M^2_{\mathrm{Pl}}} \tag{3}$$

where

$$\beta(a) = 1 + 2H(a)r_c\left(1 + \frac{\dot{H}(a)}{3H^2(a)}\right) \quad (4)$$

In an *N*-body simulation of DGP this equation is solved at every time-step to determine the fifth-force $\frac{1}{2}\nabla\phi$ which is needed to propagate the particles using the geodesics equation

$$\ddot{\mathbf{x}} + 2H\dot{\mathbf{x}} = -\frac{\nabla\Phi}{a^2} = -\frac{\nabla\Phi_N}{a^2} - \frac{\nabla\phi}{2a^2} \quad (5)$$

The original DGP model, which has self-accelerating cosmological solutions, is ruled out by observations and by problem of the ghost in the gravitational sector (Maartens & Koyama 2010). The model we study here is the so-called normal-branch DGP model where the acceleration of the Universe is driven by a cosmological constant just as in ΛCDM. This model is a useful toy-model to study the particular screening mechanism, the so-called Vainshtein mechanism (Vainshtein 1972), used by DGP to hide the modifications of gravity in local experiments. The modifications of gravity in the vicinity of a massive object of mass M are determined by a scale known as the Vainshtein radius which for DGP is given by $r_V = \left(\frac{16r_c^2GM}{9\beta^2}\right)^{1/3}$. Test-particles outside the Vainshtein radius will feel a modified gravitational force, $F_{\rm eff} = F_N\left(1 + \frac{1}{3\beta(a)}\right)$, while test-particles far inside the Vainshtein radius will just feel the standard Newtonian gravitational force.

2.2 The symmetron model

The symmetron model was originally proposed in Hinterbichler & Khoury (2010) (see also Olive & Pospelov (2008); Pietroni (2005)). The action of the symmetron model is given by

$$S = \int\sqrt{-g}\mathrm{d}^4x\left[\frac{M_{\rm Pl}^2}{2}R - \frac{1}{2}\nabla_a\phi\nabla^a\phi - V(\phi)\right] + S_M(\tilde{g}_{ab},\psi)\,, \quad (6)$$

where R is the Ricci scalar, the Einstein and Jordan frame metrics (g_{ab} and $\tilde{g}_{ab}$) are conformally related

$$\tilde{g}_{ab} = A^2(\phi)g_{ab}, \quad (7)$$

and S_M is the matter action which describes the evolution of the matter fields ψ. The potential and conformal factor that define the model are

$$V(\phi) = -\frac{1}{2}\mu^2\phi^2 + \frac{1}{4}\lambda\phi^4 + V_0 \quad (8)$$

$$A(\phi) = 1 + \frac{1}{2}\left(\frac{\phi}{M}\right)^2, \quad (9)$$

where μ and M are mass scales, λ is a dimensionless constant, and V_0 is set to match the observed cosmological constant. The equation of motion for the scalar field that comes out from the action (assuming non-relativistic matter) is

$$\Box\phi = \frac{dV(\phi)}{d\phi} + \frac{dA(\phi)}{d\phi}\rho, \quad (10)$$

By fixing the metric to be a perturbed Friedmann-Robertson-Walker metric in the Newtonian gauge

$$\mathrm{d}s^2 = -(1+2\Phi)dt^2 + a^2(1-2\Phi)(\mathrm{d}x^2 + \mathrm{d}y^2 + \mathrm{d}z^2), \quad (11)$$

where Φ is a scalar perturbation (i.e. the gravitational potential in a classical context), we can write the equation of motion of the scalar field in the form

$$\nabla^2\phi = \left(\frac{\rho}{M^2} - \mu^2\right)\phi + \lambda\phi^3 = \frac{dV_{\rm eff}(\phi)}{d\phi}, \quad (12)$$

where ρ is the matter density and the effective potential is given by

$$V_{\rm eff}(\phi) = \frac{1}{2}\left(\frac{\rho}{M^2} - \mu^2\right)\phi^2 + \frac{1}{4}\lambda\phi^4 + V_0. \quad (13)$$

Note that we have used the approximation $|A(\phi) - 1| \ll 1$ to simplify the equation above. From this equation, it is possible to see that the expectation value of the scalar field vanishes at high matter densities. This sets the conformal factor A to unity and thus decouples the scalar from the matter, producing the screening of the fifth force.

To express the equation of motion in a simple form we define a dimensionless scalar field $\chi \equiv \phi/\phi_0$, where ϕ_0 is the expectation value for $\rho = 0$:

$$\phi_0 = \frac{\mu}{\sqrt{\lambda}}. \quad (14)$$

We also substitute the three free parameters (M, μ, λ) and use instead the range of the field that corresponds to $\rho = 0$,

$$\lambda_0 = \frac{1}{\sqrt{2}\mu}\,, \quad (15)$$

a dimensionless coupling constant,

$$\beta_s = \frac{\phi_0 M_{\rm Pl}}{M^2}\,, \quad (16)$$

and the scale factor at the time of symmetry breaking,

$$a_{\rm SSB}^3 = \frac{\rho_0}{\rho_{\rm SSB}} = \frac{\rho_0}{\mu^2M^2}\,, \quad (17)$$

where $\rho_0 = 3\Omega_m H_0^2 M_{\rm Pl}^2$ is the background density at $z = 0$. We also define the associated redshift $z_{\rm SSB} = 1/a_{\rm SSB} - 1$ which is the redshift for which the modifications of gravity start to kick in cosmologically. With these variables the equation for the dimensionless scalar field χ is then

$$\nabla^2\chi = \frac{a^2}{2\lambda_0^2}\left[\left(\frac{\rho}{\rho_{\rm SSB}} - 1\right)\chi + \chi^3\right]. \quad (18)$$

The effects of the scalar field on the matter distribution in a cosmological *N*-body simulation will be given by a modification of the geodesics equation, which takes the following form:

$$\ddot{\mathbf{x}} + 2H\dot{\mathbf{x}} + \frac{\nabla\Phi}{a^2} + \frac{6\Omega_m H_0^2}{a^2}\frac{(\beta_s\lambda_0)^2}{a_{\rm SSB}^3}\chi\nabla\chi = 0. \quad (19)$$

Here H_0 is the Hubble parameter at redshift $z = 0$, Ω_m is the mean matter density at redshift $z = 0$ normalised to the critical density, and the dots represent derivatives with respect to Newtonian time defined by equation 11.

2.3 The $f(R)$ model

Among the large number of $f(R)$ models that exist in the literature we choose the well known Hu-Sawicky model presented in Hu & Sawicki (2007). The action that defines the model is

$$S = \int\sqrt{-g}\mathrm{d}^4x\left[\frac{R + f(R)}{16\pi G} + L_M\right], \quad (20)$$

where the free function f is chosen as

$$f(R) = -m^2\frac{c_1(R/m^2)^n}{c_2(R/m^2)^n + 1}, \quad (21)$$

where $m^2 \equiv H_0^2\Omega_m$ and c_1, c_2, and n are dimensionless model parameters. By requiring the model to give dark energy, it is possible to reduce the number of free parameters from three to two (n

and f_{R0}). This requirement translates into

$$\frac{c_1}{c_2} = \frac{6\Omega_\Lambda}{\Omega_m}, \tag{22}$$

where Ω_Λ is the density parameter associated with the cosmological constant. Instead of using c_1 (or c_2) as the second free parameter, it is convenient to use

$$f_{R0} = -n\frac{c_1}{c_2^2}\left(\frac{\Omega_m}{3(\Omega_m + 4\Omega_\Lambda)}\right)^{n+1}, \tag{23}$$

which relates to the range of fifth force in the cosmological background at redshift $z = 0$ as

$$\lambda_0 = 3\sqrt{\frac{(n+1)}{\Omega_m + 4\Omega_\Lambda}}\sqrt{\frac{|f_{R0}|}{10^{-6}}} \ \ \mathrm{Mpc}/h, \tag{24}$$

where λ_0 is the range of the field, which is typically given in Mpc$/h$. General Relativity is formally recovered in the limit $f_{R0} \to 0$.

In the quasi-static limit (Bose et al. 2015), the scalar field f_R fulfils the following equation of motion,

$$\nabla^2 f_R = -\tfrac{1}{a}\Omega_m H_0^2 \delta + a^2 \Omega_m H_0^2 \times \\ \times \left[\left(1 + 4\tfrac{\Omega_\Lambda}{\Omega_m}\right)\left(\tfrac{f_{R0}}{f_R}\right)^{\frac{1}{n+1}} - \left(a^{-3} + 4\tfrac{\Omega_\Lambda}{\Omega_m}\right)\right], \tag{25}$$

where $f_{R0} = f(R_0)$, R_0 is the present value of the Ricci scalar in the cosmological background and δ is the local matter overdensity in units of the mean density of the Universe.

The geodesic equation takes the form

$$\ddot{\mathbf{x}} + 2H\dot{\mathbf{x}} + \frac{\nabla\Phi}{a^2} - \frac{1}{2}\frac{\nabla f_R}{a^2} = 0, \tag{26}$$

where the last term corresponds to the fifth force.

2.4 Quintessence models

Quintessence coupled dark energy (cDE) has been proposed by several authors (e.g. Wetterich 1995; Zlatev et al. 1999; Amendola 2000) as an alternative to the standard ΛCDM, in an attempt to solve the so called fine tuning and coincidence problems of the model. These theories feature a scalar field ϕ[1] which can be non-minimally coupled to the dark matter, effectively acting as a fifth-force on DM particles. The general Lagrangian for this class of theories reads:

$$L = \int \mathrm{d}^4x\sqrt{-g}\left(-\frac{1}{2}\partial_\mu\partial^\mu\phi + V(\phi) + m(\phi)\psi_m\bar{\psi}_m\right) \tag{27}$$

where the matter field ψ_m is allowed to interact with ϕ through the $m(\phi)$, the mass term. A popular choice for the self interaction potential $V(\phi)$ is of the inverse power-law kind (Ratra & Peebles 1988):

$$V(\phi) = V_0\left(\frac{\phi}{M_p}\right)^{-\alpha} \tag{28}$$

while the mass-mediated interaction term is chosen

$$m(\phi) = m_0 \exp\left(\beta(\phi)\frac{\phi}{M_p}\right) \tag{29}$$

[1] Here and above $\phi = \phi(a)$ denotes the cosmological value of the field ϕ.

Table 1. Model parameters for the symmetron, $f(R)$, DGP and cDE runs. The range of the field in the $f(R)$ model, λ_0, is derived from the value of f_{R0} and is given in h^{-1} Mpc.

Model	β_s	z_{SSB}	λ_0 (h^{-1} Mpc)
SymmA	1	1	1
SymmB	1	2	1
Model	n	$\lvert f_{R0}\rvert$	λ_0 (h^{-1} Mpc)
FofR04	1	10^{-4}	23.7
FofR05	1	10^{-5}	7.5
FofR06	1	10^{-6}	2.4
Model	r_cH_0	r_c (h^{-1}Gpc)	
DGP12	1.2	3.6	
DGP56	5.6	16.8	
Model	α	β_0	
cDE	-0.137	0.099	

Table 2. Simulation settings for the various models. Box-sizes are expressed in units of h^{-1} Mpc.

Model	Box	N_{part}
ΛCDM-I	250	512^3
FofR04	250	512^3
DGP12	250	512^3
DGP56	250	512^3
ΛCDM-II	256	512^3
FofR05	256	512^3
FofR06	256	512^3
SymmA	256	512^3
SymmB	256	512^3
ΛCDM-III	250	2×1024^3
cDE	250	2×1024^3

In the following analysis, we will consider a simple realisation of this coupled dark energy model (cDE) with a constant $\beta(\phi) = \beta_0$ and a positive α for the potential.

3 SIMULATIONS

Simulating a fifth-force kind of interaction requires modifying standard *N*-body solvers. Here we will briefly resume the main ideas and properties of such codes. We considered a total of three simulation series, each one of which has been ran with the same initial random seed and a realization of the ΛCDM cosmology, which is

Table 3. Cosmological parameters used for the different realisations of ΛCDM.

Model	Ω_Λ	Ω_M	h	σ_8
ΛCDM-I	0.733	0.267	0.719	0.8
ΛCDM-II	0.65	0.35	0.65	0.8
ΛCDM-III	0.73	0.27	0.70	0.8

used as a benchmark. Halo catalogues have been extracted using the AHF halo finder (Knollmann & Knebe 2009). In all the ΛCDM and cDE simulations, the power spectrum of the initial conditions were normalised using the redshift zero σ_8. For $f(R)$, symmetron and DGP models the σ_8 was normalized to be the same at the *starting* redshift, leading to slightly higher $z = 0$ results. However, these small changes are not expected to play any substantial role at the sub-megaparsec scales considered in this analysis.

3.1 DGP, symmetron and f(R)

The simulations were run with the code ISIS (Llinares et al. 2014) which is a modified gravity modification of RAMSES (Teyssier 2002). The code is a particle mesh code which includes adaptive mesh refinements. In order to solve the equations for the scalar field, the code uses a non-linear version of the linear multigrid solver in RAMSES. The solver works by doing Gauss-Seidel iterations on the discretised version of the equations to find improved solutions based on an initial guess. Given the multiscale properties of the problem, the solver also uses the multigrid method to increase the speed of convergence. In these simulations we used a coarse-level grid with 512^3 grid cells and each cell was refined if the number of particles contained in it exceeded 8. The maximum refinement-level obtained in the simulations was 6 corresponding to a smallest gridcell of size $7.6 - 7.8\ h^{-1}\,\mathrm{kpc}$. Table 1 summarises the model parameters for the modified gravity theories. All the simulations were run using the same initial conditions. This is valid since at early times $z \lesssim 2$ the modifications of gravity, in all of the models simulated, have very little impact on the growth of structures.

To generate the only set of initial conditions we used the package COSMICS (Bertschinger 1999). Two box sizes have been used for these simulations, of 256 and $250h^{-1}\,\mathrm{Mpc}$, while the number of DM particles is 512^3.

The background cosmology is also the same for all the simulations and is defined as a flat ΛCDM, for which two realizations (one for each box size) have been run using the parameters shown in Table 3. All the simulations have the same normalisation. The simulations were run up to redshift zero. Furthermore, all the simulations use the same background cosmology with exactly the same initial conditions. The samples used for the analysis include all the halos reported by the halo finder with no discrimination between virialized and non-virialized objects. The halo catalogue has a cut-off for low-mass halos at 20 particles per halo, which corresponds to a minimum halo mass of $1.85 \times 10^{11} h^{-1}\mathrm{M}_{\odot}$.

3.2 Quintessence

The code used to simulate coupled quintessence was described in Carlesi et al. (2014a), and implements the algorithm of Baldi et al. (2010) on the publicly available code GADGET2 (Springel 2005).

The values for α and β_0 shown in Table 1 are chosen in order to be in agreement with WMAP7 (Pettorino et al. 2012) constraints. The simulations were ran in a $250h^{-1}\,\mathrm{Mpc}$ side periodic box using 2×1024^3 both baryonic and DM particles, with a softening length of $8\ h^{-1}\,\mathrm{kpc}$ for DM and baryonic particles. The adiabatic approximation was used for the baryonic SPH solver. As for the previous cases, along with cDE we also simulate a standard ΛCDM cosmology set up with the identical random phase for the generation of the initial condition, which enables us to consistently cross-correlate objects among the different models.

The algorithm used in the modified code is based on the standard *Tree-PM*, modified in order to take into account long-range interactions mediated by the scalar field, which affect the DM particles only. This interaction turns out to act effectively as a rescaling of the gravitational constant, which can be written as

$$G_{\mathrm{DM}}^{\mathrm{eff}} = G_N(1 + 2\beta^2(\phi)),$$

where G_N takes the standard Newtonian value. Moreover, we need to take into account the effect of cosmic friction, which is an additional quintessence mediated force proportional to $\beta(\phi)\overrightarrow{v}$. The factors above require to compute the solution of the Green functions separately for each kind of particle (whether baryonic or DM), as the additional dark energy interaction may or may not be present. The code uses a set of pre-computed tables of quantities such as the Hubble function $H(a)$, which are then read and interpolated at run time. This saves computational time, sparing the need to solve complex systems of equations on the fly at each time step. Initial conditions have been generated using a suitably modified version of the N-GenIC code [2].

4 METHODS

The analysis presented here relies on the concept of the *Local Group model*, formalized by Carlesi et al. (2016b) in the context of LG constrained simulations (Carlesi et al. 2016). In this approach, the properties that are used to select LG-like objects in cosmological simulations are explicitly treated as Bayesian priors, expressing our previous knowledge and our prejudices on the system at hand. In principle, the number of variables that can be used in the definition of the LG and its members is potentially infinite: besides mass, position and velocity, other properties can be employed, such as stellar mass (Guo et al. 2015), dwarf galaxies (Busha et al. 2011; Boylan-Kolchin et al. 2013), Hubble flow (Karachentsev et al. 2009), filamentary environment (Libeskind et al. 2015; Carlesi et al. 2016). Therefore, any LG definition of is to some extent arbitrary. This is why we emphasize here the role played by our choice of the variables used to define it. Such choices need to be flexible enough to build statistically significant samples of objects that, by some metric, are akin to the real LG. These samples can be used to produce the PDFs of LG-related variables and their combinations. In Bayesian terms, these are conditional probabilities, i.e. functions that express our expectation about a given variable assuming a specific prior model for both cosmology and the LG.

4.1 The Local Group model

The use of a LG model allows us to interchange cosmological models and LG definitions, in order to highlight the role played by cosmology in shaping the expected properties of LG-like objects. In this way, we estimate how frequently within a given theory we expect to observe *actual* values of LG-variables such as the radial velocity (v_{rad}) between MW and M31. Moreover, consistency with the actual LG can be analysed from the viewpoint of quantities such as energy and angular momentum, which due to the isolation of the system are thought to be almost exactly conserved (Forero-Romero et al. 2013). This amounts at determining whether a given cosmology may give rise (and at what rate) to perturbations that can later

[2] http://wwwmpa.mpa-garching.mpg.de/gadget/right.html#ICcode

Table 4. Kinematic priors on velocities ($v_{\rm tan}$ and $v_{\rm rad}$, in km s^{-1}), relative distances r of the haloes (in $h^{-1}\,{\rm Mpc}$) and masses (in $10^{12}h^{-1}{\rm M}_{\odot}$ units). The first set Mod0 is very broad and can be used to derive PDFs for all of the variables, assuming almost no prior knowledge of the mass, separation and $v_{\rm rad}$. In Mod1 we include LG-like objects with negative $v_{\rm rad}$ only, also restricting r and $M_{\rm LG}$ values. Mod2 and Mod3 define objects whose dynamics is within $\pm 2\sigma$ from the values of r, $v_{\rm rad}$ and $M_{\rm LG}$ of van der Marel et al. (2012); while using $\pm 1\sigma$ intervals around the $v_{\rm tan}$ values of Sohn et al. (2012) ($v_{\rm tan}^{(I)}$) and Salomon et al. (2016) ($v_{\rm tan}^{(II)}$).

	$v_{\rm rad}$	$v_{\rm tan}$	r	$M_{\rm LG}$
Mod0	$[-500, 500]$	$[0, 500]$	$[0.25, 1.50]$	$[1, 10]$
Mod1	$[-500, 0]$	$[0, 500]$	$[0.25, 0.78]$	$[1, 5]$
Mod2	$[-125, -95]$	$[0, 34]$	$[0.44, 0.60]$	$[1, 5]$
Mod3	$[-125, -95]$	$[100, 225]$	$[0.44, 0.60]$	$[1, 5]$

Table 5. Number of selected LG-like pairs per simulation. $N_{\rm Mod0}$, $N_{\rm Mod1}$, $N_{\rm Mod2}$ and $N_{\rm Mod3}$ correspond to the sample size of pairs that satisfy the kinematic priors shown in Table 2. While within some cosmologies Mod2 LGs are found at a rate comparable with ΛCDM, SymmA, SymmB, FofR04 and FofR05 are largely incapable of accounting for that kind of dynamics.

Model	$N_{\rm Mod0}$	$N_{\rm Mod1}$	$N_{\rm Mod2}$	$N_{\rm Mod3}$
ΛCDM-I	7041	1452	15	18
FofR04	6770	1373	3	7
SymmA	8290	1656	3	20
SymmB	8168	1620	0	2
ΛCDM-II	8929	1858	19	33
FofR05	9278	1792	6	35
FofR06	9877	1969	12	32
DGP12	8827	1768	19	34
DGP56	8827	1875	16	38
ΛCDM-III	7633	1738	15	30
cDE	7143	1554	10	29

evolve into an LG-kind of object. This approach and the results derived from it are discussed in Section 5.2. We stress again that computing the above quantities we treat haloes as point-like particles. Therefore, concerns about the limited resolution of the simulations are secondary here, as the internal structure of the haloes plays a substantially negligible role, as discussed in Appendix A in more detail. This has been tested using ΛCDM simulations with the same box size but with different numbers of particles. In fact, it can be shown that both the total number of LG-like pairs and the distribution functions of their properties, within the mass ranges which are relevant for the present study, are not affected nor biased by the resolution.

4.2 Implementation

We start defining a LG-like object as a pair of isolated haloes. This requirement is motivated by the fact that the mass budget of the real LG is dominated by the total mass of MW and M31. Isolation is defined as the absence of a third object of mass larger or equal than the one of the smallest halo of the pair within a radius of $2.5h^{-1}\,{\rm Mpc}$ from the centre of mass of the system. On top of these two general criteria, a series of priors on the velocities, masses and separations among these objects are imposed, gradually restricting the range of variation of such parameters to enforce a stricter resemblance to the real observed system. Table 4 shows the four ranges of these priors, which define our LG models. Mod0 is a very general model, where broad criteria are imposed to define LGs from the global number of isolated pairs. This sample is useful to study *all* the kinematic variables of the system, assuming a very superficial knowledge of the same. In other words, it can be used to answer the question: *what kind of dynamics do we expect from a pair of close-by, isolated haloes, within a given cosmological framework?*.

On the other hand, a more realistic LG model needs to reflect some more important facts about the nature of the M31-MW pair. This is done within Mod1, which implements a more detailed knowledge of the system into the priors. In this model $v_{\rm rad}$ is constrained to negative values, the range of values for $M_{\rm LG}$ and r are reduced, while keeping the number of object large enough to be statistically significant, as shown in Table 5. Such a definition overlaps with to the ones used e.g. by Forero-Romero et al. (2013); González et al. (2014); Sawala et al. (2014); Libeskind et al. (2015) and Carlesi et al. (2016).

The last two models, Mod2 and Mod3, identify *realistic* LGs, i.e. objects whose mass, velocity and separation values fall within 2σ from the observational data (van der Marel et al. 2012). Each model implements one of the conflicting measures existing for the tangential velocity of M31: a low-$v_{\rm tan}$ one, taken from Sohn et al. (2012) and referred to as $v_{\rm tan}^{(I)}$, and a high-$v_{\rm tan}$ obtained by Salomon et al. (2016) ($v_{\rm tan}^{(II)}$ hereafter). In the following sections, we will take a closer look at the kinematics and dynamics of the LG using samples drawn from each simulation using these models.

5 LG DYNAMICS

We will now study three aspects of the LG dynamics in order to present a comprehensive picture of the possible observational signatures that characterize the models under analysis. First, we will look at compatibility with observational data, counting the number of halo pairs whose properties fall within the allowed confidence intervals. This enables us to evaluate and compare the expected rate of formation of LGs in a non standard model and in ΛCDM, in a very straightforward way. Second, using a more general LG model yielding larger samples, we compute distribution functions for masses and velocities. These PDFs are then used to compute the average expected dynamics within each model, establishing a link between this cosmology and properties on astrophysical scales. As a last step, we will look at the semi-conserved quantities of the system, energy and angular momentum, to reduce the influence of transient factors that could affect the previous results.

5.1 Realistic local groups

We define as realistic LGs those halo pairs whose values of r, $v_{\rm rad}$ and $M_{\rm LG}$ fall within 2σ from the values of van der Marel et al. (2012). On top of these, we use two different 1σ priors for $v_{\rm tan}$: Mod2 implements the $v_{\rm tan}^{(I)}$ measurement of Sohn et al. (2012) while Mod3 employs the $v_{\rm tan}^{(II)}$ value of Salomon et al. (2016). The objects obtained in this way provide the most accurate representation of a LG in a simulation. However, the narrow

Table 6. Peak likelihood values for masses ($\log_{10}$ in $h^{-1}\mathrm{M}_{\odot}$ units) and velocities (km s^{-1}) for each cosmology using different LG models, together with their 95% confidence intervals. Distributions relative to the Mod2 and Mod3 samples are not shown due to the smallness of the sample size in both cases.

	Mod0			Mod1		
Model	$M_{\rm LG}$	$v_{\rm rad}$	$v_{\rm tan}$	$M_{\rm LG}$	$v_{\rm rad}$	$v_{\rm tan}$
ΛCDM-I	12.44 ± 0.30	-101^{+40}_{-54}	72^{+48}_{-30}	12.35 ± 0.20	-124^{+36}_{-40}	78^{+44}_{-33}
FofR04	12.45 ± 0.30	-118^{+49}_{-66}	92^{+63}_{-41}	12.35 ± 0.20	-150^{+51}_{-70}	98^{+55}_{-41}
SymmA	12.46 ± 0.29	-114^{+45}_{-58}	74^{+52}_{-32}	12.35 ± 0.21	-153^{+45}_{-44}	82^{+54}_{-33}
SymmB	12.45 ± 0.31	-144^{+59}_{-78}	95^{+65}_{-42}	12.35 ± 0.22	-198^{+69}_{-65}	113^{+63}_{-49}
ΛCDM-II	12.36 ± 0.32	-90^{+39}_{-55}	69^{+46}_{-29}	12.30 ± 0.22	-121^{+40}_{-42}	79^{+43}_{-33}
FofR05	12.36 ± 0.32	-106^{+46}_{-64}	82^{+58}_{-46}	12.32 ± 0.23	-145^{+47}_{-55}	95^{+54}_{-39}
FofR06	12.38 ± 0.33	-103^{+44}_{-60}	75^{+52}_{-32}	12.32 ± 0.23	-141^{+43}_{-49}	89^{+51}_{-39}
DGP12	12.36 ± 0.33	-92^{+40}_{-58}	73^{+51}_{-31}	12.30 ± 0.22	-123^{+40}_{-43}	78^{+47}_{-33}
DGP56	12.36 ± 0.32	-91^{+41}_{-55}	69^{+48}_{-28}	12.29 ± 0.22	-120^{+38}_{-45}	79^{+46}_{-34}
ΛCDM-III	12.46 ± 0.26	-96^{+44}_{-57}	70^{+53}_{-34}	12.38 ± 0.17	-120^{+39}_{-44}	77^{+50}_{-37}
cDE	12.46 ± 0.28	-112^{+48}_{-59}	82^{+56}_{-36}	12.38 ± 0.17	-149^{+43}_{-42}	89^{+54}_{-37}

interval of values due to such strict definitions does not allow to gather statistically meaningful halo samples. Therefore, to obtain an estimate of the viability of a theory we will simply refer to the number of objects complying with these two prior models.

In the last two columns of Table 5, it is shown how the Mod2 and Mod3 sample sizes are affected by a change of the cosmology. In the cases of cDE, FofR06 DGP12 and DGP56 we see that (for both Mod2 and Mod3) these numbers do not substantially change in comparison to the benchmark ΛCDM-I, ΛCDM-II and ΛCDM-III simulations. This means that the aforementioned models are able to reproduce object whose dynamics is compatible with the one observed for the actual LG *at least at the same rate* of ΛCDM. However, the other models show a different behaviour. In particular, it has be be noticed how implementing a low-$v_{\rm tan}$ prior the number of haloes found within the FofR04, FofR05, SymmA and SymmB simulations is drastically reduced, indicating that this specific kind of dynamics can hardly be accounted for within those cosmological frameworks. Most notably, the SymmB model has no Mod2-complying pairs, in SymmA and FofR04 the number is reduced five-fold and in FofR05 three-fold. When assuming a high-$v_{\rm tan}$ prior, on the other hand, the number of objects reaches ΛCDM levels in SymmA and FofR05 and is increased in both FofR04 and SymmB indicating that $v^{(I)}_{\rm tan}$ yields more constraining power than $v^{(II)}_{\rm tan}$.

5.2 Kinematic variables

Local group masses Masses for the LG and its two main haloes are not affected by the change in cosmology. Table 6 shows that for in each simulation both the peak likelihood and the scatter for the $\log_{10}M_{\rm LG}$ distributions are sensitive to the LG model only and are not affected by modified gravity and cDE. A small reduction in the mass can be seen on average when switching from Mod0 to Mod1, that is, when selecting pairs with strictly negative $v_{\rm tan}$. Individual masses and the $M_{\rm MW}$ to $M_{\rm M31}$ ratios are also not affected. We therefore conclude that the mass of the local group and of its members cannot be used as a probe for the kinds of alternative theories considered. In the case of cDE, this finding is consistent with Penzo et al. (2015) who found a weak dependence of $M_{\rm vir}$ on the cosmology and cam be expected from the negligible changes to the halo mass function associated with this kind of DE model (see Macciò et al. 2004; Baldi et al. 2010; Cui et al. 2012; Carlesi et al. 2014a).

Radial and tangential velocity Factoring the mass parameter out of the following analysis, we seek to establish a direct link between alternative models and expected LG kinematics. Pairwise velocity has been shown to be strongly affected in modified gravity models by Hellwing et al. (2014), so that we expect some correlation between $v_{\rm rad}$, $v_{\rm tan}$ and modifications to GR. In Fig. 1 we show the peaks of the likelihood in the $v_{\rm rad}$- $v_{\rm tan}$ plane for the Mod0 and Mod1 samples, with error bars and shaded regions indicating the 95% confidence level for models' estimates and observations. First of all, we remark how the three ΛCDM simulations largely agree with each other and with the results of Forero-Romero et al. (2013) and Carlesi et al. (2016b), indicating that the cosmic variance and the different cosmological parameters play here a negligible role. This is true for both Mod0 and Mod1 ΛCDM samples, so that we can conclude that the reduction in sample size does not affect our results at this stage. From both panels we observe that the different cosmologies can predict several kinds of dynamics overlapping in some cases only at the two sigma level. However, these differences are enhanced in Mod1 that comprises a more realistic LG-like kind of objects, i.e. those pairs with negative radial velocity. In this case we can see how all of the cosmologies, except for DGP which closely mimics ΛCDM, are characterized by peak $v_{\rm tan}$ values substantially larger in module than the observational interval. In particular, SymmB does not overlap with the allowable range of values, meaning that the likelihood of observing a combination of velocities compatible with the LG would is less than 5%. Moreover, also SymmA, cDE, FofR04, FofR05 and FofR06 cannot reproduce the data, preferring $v_{\rm rad}$- $v_{\rm tan}$ combinations that only marginally agree with the observations. In table Table 6 these values are shown together with their ΛCDM counterparts: we can see how the additional interaction affects the peaks, increasing the absolute value of $v_{\rm tan}$ by $\approx 60\%$ and $v_{\rm rad}$ by $\approx 50\%$ in SymmB. These same values $\approx 20-30\%$ larger in the case of the other $f(R)$ and symmetron models. This enhancement is due to the additional interaction and is proportional to the strength of the coupling, as can be seen in the case of $f(R)$. We have thus been able to de-

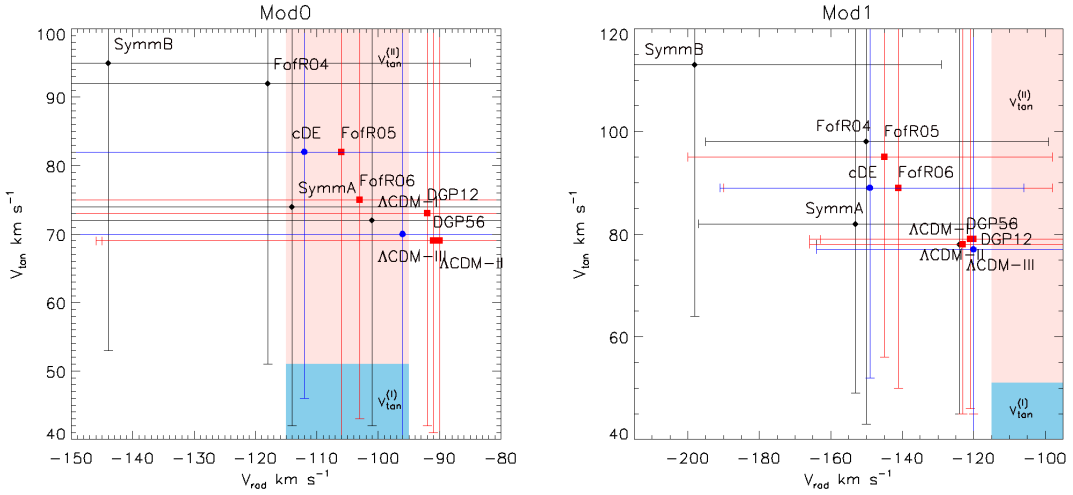

Figure 1. Peak values of $v_{\rm tan}$ versus $v_{\rm rad}$ for the different cosmologies and the two LG models Mod0, Mod1, together with their 95% confidence level values. The shaded regions stretch horizontally for on very narrow interval of values, due to the precision of the $v_{\rm rad}$ measurements. On the other hand, conflicting $v_{\rm tan}$ measurements lead to a much larger range of 95%-allowable values on the y axis. Models such as SymmB can be seen to predict a combination of velocities outside the region allowed by actual measurements.

Table 7. Values and intervals used to generate MC contours. $M_{\rm MW}$, $M_{\rm M31}$ are expressed in $10^{12}h^{-1}{\rm M}_{\odot}$ units, inter halo distance r in h^{-1} kpc while $v_{\rm rad}$ and $v_{\rm tan}$ in km s^{-1}. The intervals on r and $v_{\rm rad}$ correspond to the 2σ values of van der Marel et al. (2012), while for $v_{\rm tan}$ they were chosen in agreement with (Sohn et al. 2012).

$M_{\rm MW}$	(0.5, 2.5)
$M_{\rm M31}$	(0.5, 2.5)
r	(440, 600)
$v_{\rm rad}$	(-125, -95)
$v_{\rm tan}$	(0, 50)

termine that the fifth-force induced modifications to the expected velocities favour kinematic configurations largely at odds with the observations. This result confirms what we had found analysing Mod2 and Mod3 samples, where the sharp reduction in the number of viable LGs in the SymmB, FofR04 and FofR05 cosmologies also signalled the difficulty of such theories to account for the real LG dynamics..

5.3 Global properties

In addition to the analysis of mass and velocity, which are directly observable and can be straightforwardly compared to the available data, it is useful to take a look at the global dynamical state of the system, determined by *combinations* of observable variables. In fact, the capacity of a given cosmological model to produce halo pairs whose properties are consistent with actual observations of r, $v_{\rm tan}$ and $v_{\rm rad}$ at $z = 0$ does not rule out the possibility that these transient values might be closer to the real LG ones in a different moment backwards or forwards in time. Therefore, a complementary approach consists in analysing combinations of variables, conveying informations about more fundamental properties of the system.

Semi-conserved quantities We start defining two quantities that characterize the *global* dynamical state of the LG. Placing ourselves in the MW frame of reference we introduce the reduced total energy:

$$e_{\rm red} = \frac{1}{2}\mathbf{v}_{\rm M31}^2 - \frac{GM_{\rm LG}}{|\mathbf{r}_{\rm M31}|} \tag{30}$$

and the (reduced) orbital angular momentum:

$$l_{\rm orb} = |\mathbf{r}_{\rm M31} \times \mathbf{v}_{\rm M31}| \tag{31}$$

Ideally, these two quantities would be perfectly conserved if the identified LG-like objects were completely isolated, in reality, interactions with smaller nearby haloes spoil their exact conservation. Moreover, it has to be noticed that Eq. (30) is derived assuming GR, and therefore is not expected to measure the total (reduced) energy within cDE and modified gravity cosmologies. However, this variable can still be used in those contexts as an *observationally*-relevant variable, putting aside its original physical meaning. In fact, Eq. (30) is a combination of astrophysical variables that do not rely on cosmology for their measurement. Our aim here is to determine how it is expected to behave in modified gravity and coupled dark energy, and compare that to observations in a consistent and model-independent approach.

To compare $e_{\rm red}$ and $l_{\rm orb}$ with the data, we follow the procedure of Forero-Romero et al. (2013), drawing contours in the $e_{\rm red}$-$l_{\rm orb}$ plane to identify those regions of the parameter space that are compatible with current observations. The contours are generated through 10^7 Monte Carlo iterations, where at each step the values of velocity, mass and distance are drawn from a Gaussian distribution within the intervals shown in Table 7. The value of $v_{\rm rad}$ was taken from van der Marel et al. (2012), r from van der Marel & Guhathakurta (2008), while $M_{\rm MW}$ and $M_{\rm M31}$ are consistent with van der Marel et al. (2012) and Boylan-Kolchin et al. (2013). Due to the large discrepancy existing among the $v_{\rm tan}^{(I)}$ and $v_{\rm tan}^{(II)}$ the MC was ran twice using the two different estimates.

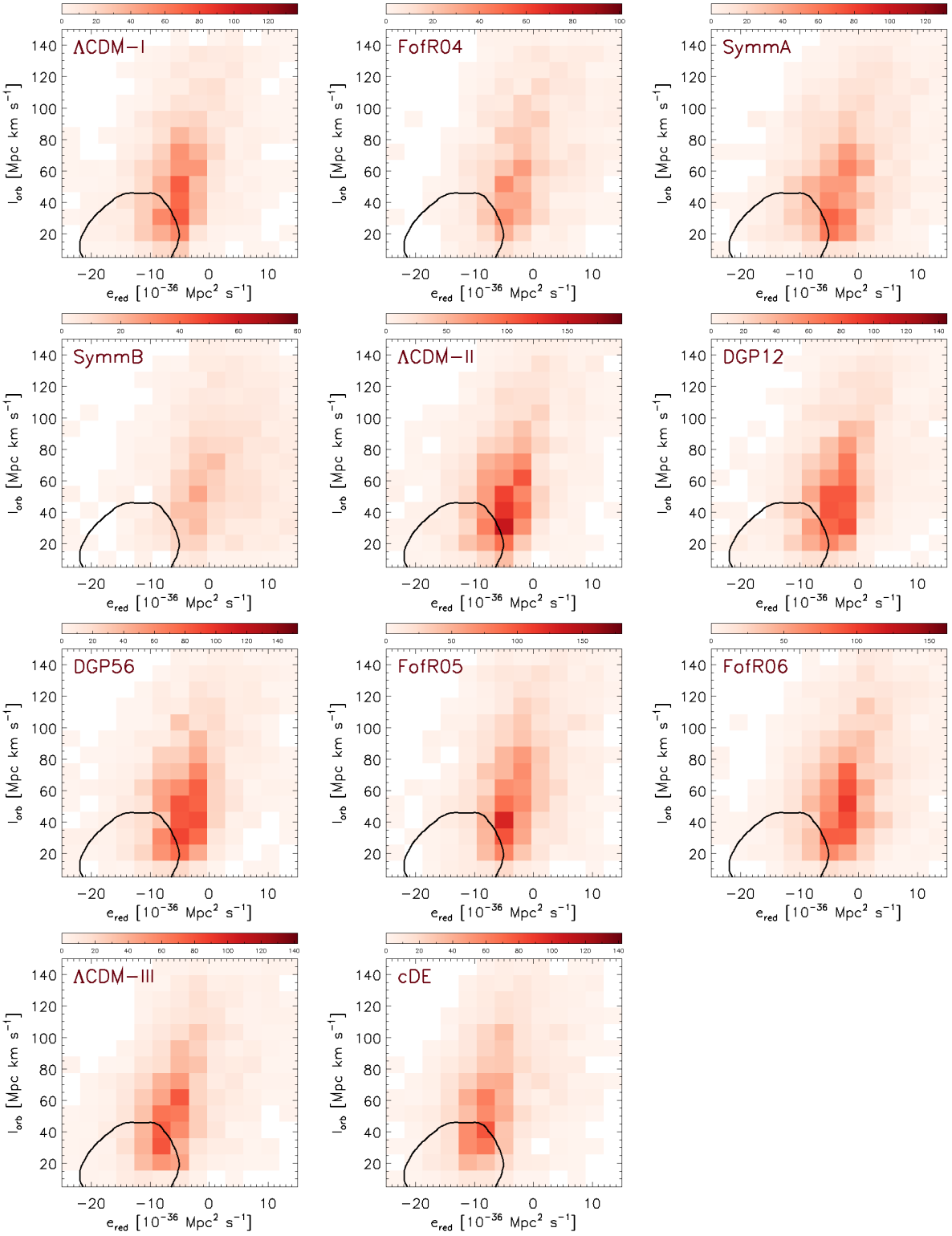

Figure 2. LG-like pairs versus MC contours showing the 1σ and 2σ confidence levels. Pairs have been chosen and MC intervals have been generated using the low $v_{\rm tan}$ estimate of (Sohn et al. 2012)

It turns out that the intervals generated with $v_{\rm tan}^{(II)}$ are extremely large and possess no constraining power, so that we do not consider them in the following analysis.

In Fig. 2 we bin the Mod1 objects in the $e_{\rm red}$ - $l_{\rm orb}$ plane and compare them to the observational 95% confidence intervals. The fraction of objects $f_{\rm LG}$ that falls within those boundaries is shown in the last column of Table 8. This quantity allows us to gauge the ability of a model to account for the observed *global* dynamics of the system disregarding its transient state. We note that the number

Table 8. Energy, angular momentum, spin parameter and fraction of Mod1 pairs falling within the 95% confidence level of the MC generated boundaries.

Model	$l_{\rm orb}$	$e_{\rm red}$	$\log_{10}\lambda$	$f_{\rm LG}$
ΛCDM-I	$53.82^{+26.06}_{-22.53}$	$-3.96^{+2.80}_{-2.89}$	$-1.49^{+0.19}_{-0.24}$	0.16
FofR04	$59.48^{+31.69}_{-24.16}$	$-1.65^{+3.83}_{-2.99}$	$-1.52^{+0.24}_{-0.27}$	0.08
SymmA	$53.21^{+29.06}_{-22.09}$	$-2.90^{+3.71}_{-3.59}$	$-1.54^{+0.21}_{-0.28}$	0.13
SymmB	$60.45^{+29.73}_{-22.74}$	$0.54^{+5.37}_{-3.64}$	$-1.59^{+0.27}_{-0.31}$	0.05
ΛCDM-II	$52.30^{+26.92}_{-21.10}$	$-3.69^{+2.59}_{-3.13}$	$-1.49^{+0.19}_{-0.26}$	0.15
FofR05	$59.49^{+28.99}_{-22.87}$	$-1.38^{+3.35}_{-2.69}$	$-1.50^{+0.23}_{-0.30}$	0.06
FofR06	$56.40^{+26.08}_{-22.01}$	$-2.25^{+3.13}_{-2.98}$	$-1.52^{+0.23}_{-0.28}$	0.09
DGP12	$53.60^{+27.50}_{-20.38}$	$-3.34^{+2.56}_{-3.14}$	$-1.48^{+0.19}_{-0.26}$	0.14
DGP56	$52.09^{+26.25}_{-20.72}$	$-3.60^{+2.46}_{-3.15}$	$-1.49^{+0.20}_{-0.26}$	0.14
ΛCDM-III	$52.11^{+25.41}_{-18.88}$	$-3.41^{+2.35}_{-2.47}$	$-1.48^{+0.23}_{-0.28}$	0.19
cDE	$56.43^{+27.96}_{-18.63}$	$-2.98^{+2.41}_{-2.36}$	$-1.59^{+0.24}_{-0.28}$	0.15

for ΛCDM varies between 0.15 and 0.19 – which is consistent with Forero-Romero et al. (2013), who found a 0.08 to 0.12 fraction at the 68% confidence interval. In the case of modified gravity cosmologies, the results largely confirm the conclusions obtained with the previous analyses of velocities. In fact, models such as FofR04, FofR05, SymmB and - to a lesser extent - FofR06 produce LG-like pairs within the observational boundaries at substantially lower rates than ΛCDM. In particular, the fraction of Mod1 LGs falling within the 95% confidence level is reduced by a factor of three in SymmB and around a factor of two in FofR04 and FofR05, showing from another perspective that the LG dynamics can only be poorly accounted for within these models. These discrepancies are explained by the increased velocity of M31, affecting the values of $e_{\rm red}$ (through the kinetic energy term in Eq. (30) and $l_{\rm orb}$, that tend to shift the distribution farther away from the region allowed by the data.

Spin parameter Besides these two variables, we conclude our analysis taking a look at the dimensionless spin parameter λ (Peebles 1971), which is defined as

$$\lambda = \frac{\mu^{3/2} l_{\rm orb}\sqrt{e_{\rm red}}}{G M_{\rm LG}^{5/2}} \tag{32}$$

where $\mu = (M_{\rm MW} M_{\rm M31})/M_{\rm LG}$ and G is the Newtonian constant. Spin parameters for individual haloes are known to be slightly higher in fifth-force cosmologies, as enhanced velocities also lead to an increased rotational support of the haloes (Hellwing et al. 2013; Carlesi et al. 2014a; He et al. 2015). This is consistent with our findings about the spin parameter distribution: in Table 8 we clearly see how the median $\log_{10}(\lambda)$ values tend to be slightly higher in cDE, $f(R)$ and Symmetron cosmologies. DGP results, on the other hand, are perfectly aligned with ΛCDM due to the negligible changes to pairwise velocities discussed above. For consistency, we have also checked that ΛCDM results for this quantities are consistent with the values found by Forero-Romero et al. (2013). However, this effect is generally rather small and does not yield much constraining power on the models.

6 CONCLUSIONS

In this work we have studied the dynamics of LG-like objects within different cosmologies. We evaluated the consistency of the observed kinematics of MW and M31 with alternative models of the Universe, in order to gauge their viability under the assumption that the LG is not an outlier - – an idea that lies at the core of the *near-field* cosmology approach. Four different kinds of alternative cosmologies were taken into account: $f(R)$ (Hu & Sawicki 2007), the symmetron (Hinterbichler & Khoury 2010), DGP (Dvali et al. 2000) and coupled quintessence (cDE, Amendola 2000). The *N*-body simulations for each model were ran using different parameters and then was compared to a benchmark ΛCDM simulation with an identical random-phase realization of the initial conditions. All of these non standard models introduce a fifth-force interaction to explain the observed late-time acceleration of the Universe, and such a modification of the standard gravitational force is expected to affect the dynamics at LG scales. Therefore, we aimed at determining how often one expects to find LG-like objects in simulations of alternative cosmological frameworks, given a definition (model) of the LG, motivated by astrophysical observations.

We identified LGs as pairs of isolated haloes, using four variables for the identification of such objects: total mass $M_{\rm LG}$, inter-halo separation r, radial velocity $v_{\rm rad}$ and tangential velocity $v_{\rm tan}$. From these four quantities, three additional variables where derived, i.e. the (reduced) total energy $e_{\rm red}$, (reduced) orbital angular momentum $l_{\rm orb}$ (both of which are almost exactly conserved and thus convey time-independent information about the system) and dimensionless spin parameter λ. All these quantities treat haloes as point-like particles, allowing us to neglect their internal structure and lowering the resolution requirements for the simulations.

We introduced four different LG models, enforcing different priors on the aforementioned variables. The samples of objects obtained in this way allowed us to carry a three-level analysis for each cosmology, focusing on

(a) 2σ-agreement with r, $v_{\rm rad}$, $M_{\rm LG}$and $v_{\rm tan}$
(b) distribution of $v_{\rm tan}$- $v_{\rm rad}$
(c) distribution of $e_{\rm red}$ and $l_{\rm orb}$

Point (a) allowed to determine of many LG-like objects could be found with a specific (transient) dynamical state in agreement with observations. In this case, and in particular using the low-$v_{\rm tan}$ estimate of Sohn et al. (2012) ($v_{\rm tan}^{(I)}$), it was possible to establish that SymmA, SymmB, FofR04 and FofR05 can hardly account for the observed properties of the LG, which cannot be reproduced at all (like in SymmB) or can be reproduced at a rate three to five

smaller than in ΛCDM (as in the case of SymmA, FofR04 and FofR05). On the other hand, high-$v_{\rm tan}$ estimates (the $v_{\rm tan}^{(II)}$ of Salomon et al. (2016)) would be in agreement with most of the models, with the exception of SymmB and FofR04.

However, to address the problems related to the transitive nature of those variables as well as the statistical significance of the samples, two additional halo samples were built using the broader selection criteria of Mod0 and Mod1 and study the variables mentioned in point (b) and (c).

We first noticed that even though different cosmologies to not change the distribution of masses, they predict a very different kind of kinematics, in particular for halo pairs with negative radial velocities. Peak values for $v_{\rm tan}$ and $v_{\rm rad}$ are up to $\approx 60\%$ than in ΛCDM for the most extreme case (SymmB), and show an average increase of $\approx 25\%$ for SymmA, FofR04, FofR05 and cDE. These deviations from the expected ΛCDM behaviour are a direct consequence of the fifth-force, which acts as an additional pull alongside gravity, enhancing the relative velocity between the halos. This picture is consistent with the results of point (c). In fact, as a consequence of higher average velocities, LG-like pairs have in general larger (less negative) $e_{\rm red}$, $l_{\rm orb}$ as well as λ values. This is more clear in the case SymmB, FofR04 and FofR05, where the large increase in the (reduced) kinetic energy term of Eq. (30) leads, in the most extreme case, to a positive median $e_{\rm red}$ of $0.54^{+5.37}_{-3.64}$, way above the quoted ΛCDM value of $-3.96^{+2.80}_{-2.89}$. Binning the number of haloes in the $e_{\rm red}$- $l_{\rm orb}$ plane, we could determine that same models lead to a fraction of LGs within the 95% observational confidence interval which is $(2-3)$ times smaller than ΛCDM. cDE, FofR06 and SymmA have similar features (of higher $e_{\rm red}$, $l_{\rm orb}$ and λ values) though the global state of the system overlaps consistently more with ΛCDM. DGP12 and DGP56 on the other hand, are indistinguishable from the standard models.

These results are consistent with other well-known probes. For the Hu-Sawicky $f(R)$ model the best constraints today from cluster abundances (Cataneo et al. 2015), and Sunyaev-Zel'dovich clusters (Peirone et al. 2016) and from the matter power-spectrum (Dossett et al. 2014)) place the FofR04 model at odds with the data and also disfavour FofR05 (see Gronke et al. 2016, for a list of other constraints). Not many groups have performed explicit analysis for the symmetron, though the enhancement of the power-spectrum and the halo mass-function (Brax et al. 2012) also show that the SymmB model is in tension with observations.

To sum up, we have analysed the small-scale regime of a large set of alternative cosmological theories, highlighting out the effects of an additional fifth-force interaction on the dynamics of the LG. Such an approach has the advantage of not requiring high-resolution simulations to deliver predictions on sub-megaparsec scales. Applying this kind of analysis to cosmological simulations, we have been able to signal a large difference between the theoretical predictions of some models and the observations. In those cases, we found that the additional pull is likely to lead to extremely large relative velocities between the main haloes of the LG, increasing its energy and angular momentum budget. We have shown that this method is capable of helping in the process of model selection using astrophysical-scale data, which, used in combination with other cosmological probes, can lead to a deeper understanding of the still unsolved mysteries of our Universe.

ACKNOWLEDGEMENTS

EC would like to thank the Lady Davis Fellowship Fund for financial support and Yehuda Hoffman for the useful discussions. He would also like to thank Roland Triay and Brent Tully for the invitation to the Cosmic Flows 2016 at the 12^{th} *Rencontres du Vietnam* conference where the idea behind this work was first discussed. HAW is supported by the Beecroft Trust. The simulations used in this paper were performed on the NOTUR cluster `HEXAGON`, the computing facilities at the University of Bergen. DFM acknowledges support from the Research Council of Norway, and the NOTUR facilities.

REFERENCES

Amendola L., 2000, Phys. Rev. D, 62, 043511
Armendariz-Picon C., Mukhanov V., Steinhardt P. J., 2000, Phys. Rev. Lett., 85, 4438
Arnold C., Puchwein E., Springel V., 2014, MNRAS, 440, 833
Baldi M., 2012, Physics of the Dark Universe, 1, 162
Baldi M., Pettorino V., 2011, MNRAS, 412, L1
Baldi M., Pettorino V., Robbers G., Springel V., 2010, MNRAS, 403, 1684
Beltrán Jiménez J., Maroto A. L., 2008, Phys. Rev. D, 78, 063005
Bertschinger E., , 1999, COSMICS: Cosmological initial conditions and microwave anisotropy codes, Astrophysics Source Code Library
Bland-Hawthorn J., Peebles P. J. E., 2006, Science, 313, 311312
Bose S., Hellwing W. A., Li B., 2015, JCAP, 2, 034
Boylan-Kolchin M., Bullock J. S., Sohn S. T., Besla G., van der Marel R. P., 2013, ApJ, 768, 140
Brax P., Davis A.-C., Li B., Winther H. A., Zhao G.-B., 2012, JCAP, 10, 002
Bull P., et al., 2016, Physics of the Dark Universe, 12, 56
Busha M. T., Marshall P. J., Wechsler R. H., Klypin A., Primack J., 2011, ApJ, 743, 40
Caldwell R. R., Dave R., Steinhardt P. J., 1998, Physical Review Letters, 80, 1582
Carlesi E., Hoffman Y., Sorce J. G., Gottloeber S., Yepes G., Courtois H., Tully R. B., 2016b, ArXiv e-prints
Carlesi E., Knebe A., Lewis G. F., Wales S., Yepes G., 2014a, MNRAS, 439, 2943
Carlesi E., Knebe A., Lewis G. F., Yepes G., 2014b, MNRAS, 439, 2958
Carlesi E., Knebe A., Yepes G., Gottlöber S., Jiménez J. B., Maroto A. L., 2011, MNRAS, 418, 2715
Carlesi E., Knebe A., Yepes G., Gottlöber S., Jiménez J. B., Maroto A. L., 2012, MNRAS, 424, 699
Carlesi E., Sorce J. G., Hoffman Y., Gottlöber S., Yepes G., Libeskind N. I., Pilipenko S. V., Knebe A., Courtois H., Tully R. B., Steinmetz M., 2016, MNRAS, 458, 900
Cataneo M., Rapetti D., Schmidt F., Mantz A. B., Allen S. W., Applegate D. E., Kelly P. L., von der Linden A., Morris R. G., 2015, Phys. Rev. D, 92, 044009
Clifton T., Ferreira P. G., Padilla A., Skordis C., 2012, Phys. Rept., 513, 1
Copeland E. J., Liddle A. R., Wands D., 1998, Phys. Rev. D, 57, 4686
Cui W., Baldi M., Borgani S., 2012, MNRAS, 424, 993
Dossett J., Hu B., Parkinson D., 2014, JCAP, 3, 046
Dvali G., Gabadadze G., Porrati M., 2000, Physics Letters B, 485, 208

Elahi P. J., Lewis G. F., Power C., Carlesi E., Knebe A., 2015, MNRAS, 452, 1341
Elyiv A., Marulli F., Pollina G., Baldi M., Branchini E., Cimatti A., Moscardini L., 2015, MNRAS, 448, 642
Falck B., Koyama K., Zhao G.-b., Li B., 2014, JCAP, 7, 058
Forero-Romero J. E., Hoffman Y., Bustamante S., Gottlöber S., Yepes G., 2013, APJL, 767, L5
González R. E., Kravtsov A. V., Gnedin N. Y., 2014, ApJ, 793, 91
Gronke M., Hammami A., Mota D. F., Winther H. A., 2016, ArXiv e-prints
Gronke M., Mota D. F., Winther H. A., 2015, A&A, 583, A123
Guo Q., Cooper A. P., Frenk C., Helly J., Hellwing W. A., 2015, MNRAS, 454, 550
Hammami A., Llinares C., Mota D. F., Winther H. A., 2015, MNRAS, 449, 3635
Harrison I., Coles P., 2011, MNRAS, 418, L20
He J.-h., Li B., Hawken A. J., 2015, Phys. Rev. D, 92, 103508
Hellwing W. A., Barreira A., Frenk C. S., Li B., Cole S., 2014, Physical Review Letters, 112, 221102
Hellwing W. A., Cautun M., Knebe A., Juszkiewicz R., Knollmann S., 2013, JCAP, 10, 012
Hinterbichler K., Khoury J., 2010, Phys. Rev. Lett., 104, 231301
Hu W., Sawicki I., 2007, Phys. Rev., D76, 064004
Kamenshchik A., Moschella U., Pasquier V., 2001, Physics Letters B, 511, 265
Karachentsev I. D., Kashibadze O. G., Makarov D. I., Tully R. B., 2009, MNRAS, 393, 1265
Khoury J., 2010, ArXiv e-prints
Knollmann S. R., Knebe A., 2009, ApJS, 182, 608
Kroupa P., Pawlowski M., Milgrom M., 2012, International Journal of Modern Physics D, 21, 1230003
Lee J., Baldi M., 2012, ApJ, 747, 45
Li B., Barrow J. D., 2011, MNRAS, 413, 262
Li B., Zhao G.-B., Teyssier R., Koyama K., 2012, JCAP, 1, 051
Libeskind N. I., Hoffman Y., Tully R. B., Courtois H. M., Pomarède D., Gottlöber S., Steinmetz M., 2015, MNRAS, 452, 1052
Llinares C., Mota D. F., 2013, Physical Review Letters, 110, 151104
Llinares C., Mota D. F., Winther H. A., 2014, Astron. Astrophys., 562, A78
Maartens R., Koyama K., 2010, Living Reviews in Relativity, 13
Macciò A. V., Mainini R., Penzo C., Bonometto S. A., 2015, MNRAS, 453, 1371
Macciò A. V., Quercellini C., Mainini R., Amendola L., Bonometto S. A., 2004, Phys. Rev. D, 69, 123516
Mota D. F., Kristiansen J. R., Koivisto T., Groeneboom N. E., 2007, Mon. Not. Roy. Astron. Soc., 382, 793
Mota D. F., Shaw D. J., Silk J., 2008, Astrophys. J., 675, 29
Olive K. A., Pospelov M., 2008, Phys. Rev. D, 77, 043524
Pawlowski M. S., Famaey B., Merritt D., Kroupa P., 2015, ApJ, 815, 19
Peebles P. J. E., 1971, A&A, 11, 377
Peirone S., Raveri M., Viel M., Borgani S., Ansoldi S., 2016, ArXiv e-prints
Penzo C., Macciò A. V., Baldi M., Casarini L., Oñorbe J., 2015, ArXiv e-prints
Penzo C., Macciò A. V., Baldi M., Casarini L., Oñorbe J., Dutton A. A., 2016, MNRAS, 461, 2490
Penzo C., Macciò A. V., Casarini L., Stinson G. S., Wadsley J., 2014, MNRAS, 442, 176
Perlmutter S., et al., 1999, ApJ, 517, 565
Pettorino V., Amendola L., Baccigalupi C., Quercellini C., 2012, Phys. Rev. D, 86, 103507
Pietroni M., 2005, Phys. Rev. D, 72, 043535
Pollina G., Baldi M., Marulli F., Moscardini L., 2016, MNRAS, 455, 3075
Puchwein E., Baldi M., Springel V., 2013, MNRAS, 436, 348
Ratra B., Peebles P. J. E., 1988, Phys. Rev. D, 37, 3406
Riess A. G., et al., 1998, AJ, 116, 1009
Salomon J.-B., Ibata R. A., Famaey B., Martin N. F., Lewis G. F., 2016, MNRAS, 456, 4432
Sawala T., Frenk C. S., Fattahi A., Navarro J. F., Bower R. G., Crain R. A., Dalla Vecchia C., Furlong M., Helly J. C., Jenkins A., Oman K. A., Schaller M., Schaye J., Theuns T., Trayford J., White S. D. M., 2014, ArXiv 1412.2748
Shi D., Li B., Han J., Gao L., Hellwing W. A., 2015, MNRAS, 452, 3179
Shim J., Lee J., Li B., 2014, ApJ, 784, 84
Sohn S. T., Anderson J., van der Marel R. P., 2012, ApJ, 753, 7
Springel V., 2005, MNRAS, 364, 1105
Sutter P. M., Carlesi E., Wandelt B. D., Knebe A., 2015, MNRAS, 446, L1
Teyssier R., 2002, A&A, 385, 337
Vainshtein A. I., 1972, Physics Letters B, 39, 393
van der Marel R. P., Fardal M., Besla G., Beaton R. L., Sohn S. T., Anderson J., Brown T., Guhathakurta P., 2012, ApJ, 753, 8
van der Marel R. P., Guhathakurta P., 2008, ApJ, 678, 187
Vargas dos Santos M., Winther H. A., Mota D. F., Waga I., 2016, A&A, 587, A132
Viel M., Markovič K., Baldi M., Weller J., 2012, MNRAS, 421, 50
Waizmann J.-C., Ettori S., Moscardini L., 2011, MNRAS, 418, 456
Wetterich C., 1995, A&A, 301, 321
Will C. M., 2014, Living Rev. Rel., 17, 4
Winther H. A., Ferreira P. G., 2015, Phys. Rev. D, 92, 064005
Winther H. A., Mota D. F., Li B., 2012, ApJ, 756, 166
Winther H. A., Schmidt F., Barreira A., Arnold C., Bose S., Llinares C., Baldi M., Falck B., Hellwing W. A., Koyama K., Li B., Mota D. F., Puchwein E., Smith R. E., Zhao G.-B., 2015, MNRAS, 454, 4208
Zlatev I., Wang L., Steinhardt P. J., 1999, Physical Review Letters, 82, 896

This paper has been typeset from a TEX/ LATEX file prepared by the author.

APPENDIX A: RESOLUTION EFFECTS ON THE DISTRIBUTIONS OF KINEMATIC PROPERTIES

The distribution functions used throughout this *paper* have been obtained using halo samples which included objects composed by a number of particles as low as ≈ 40. In the present appendix we will show that the poor resolution of some haloes does not systematically bias our results, by comparing the changes induced to

- the number of objects as a function of the model
- the distribution of $v_{\rm tan}$
- the distribution of $v_{\rm rad}$
- the distribution of total local group mass
- the distribution of mass ratios

Table A1. Parameter intervals for the two Local Group models for the test simulations; $v_{\rm rad}$ and $v_{\rm tan}$ values are expressed in km s^{-1}, r in h^{-1} kpc and $M_{\rm LG}$ in $10^{12}h^{-1}{\rm M}_{\odot}$ units.

	$v_{\rm rad}$	$v_{\rm tan}$	r	$M_{\rm LG}$
Model0	[-125, -95]	[0, 500]	[0.44, 0.60]	[0.5, 2]
Model1	[-500, -0]	[0, 500]	[0.25, 1.50]	[0.5, 7]

Table A2. Number of LG-like candidates as a function of model and realisation.

	256^3	$512^3(a)$	$512^3(b)$
N (SimuI, Model0)	26	26	16
N (SimuI, Model1)	669	663	660
N (SimuII, Model0)	18	20	21
N (SimuII, Model1)	652	714	668

by changing the particles' mass. For this aim, we use a series of pure DM ΛCDM simulations, within a $100h^{-1}\,{\rm Mpc}$ box and with Planck-I parameters, which were previously ran for testing purposes within the context of the Local Group Factory pipeline (Carlesi et al. 2016). We start with two 256^3 particle simulations, SimuI and SimuII, with a mass resolution of $5.26\times10^9h^{-1}{\rm M}_{\odot}$. For consistency reasons, we introduce two different LG models (shown in Table A1); in this way the smallest haloes in the sample will be resolved with the same number of particles as the ones previously used.

Then, for each simulation, we generate two sets of initial conditions with 512^3 particles, for a total of four higher resolution realisations. The first two of them share the same SimuI random phases on a 256^3 grid, but use different phases for the generation of the white noise on the smaller scales. The second pair is generated in the same manner, on top of the SimuII white noise field. This setting allows use to single out resolution effects from those induced by large-scale and small-scale cosmic variance.

We use two Local Group Models, a restrictive one (Model0) and a second one with broader intervals (Model1), specified in Table A2. The first one will allow us to evaluate resolution effects on small halo samples, whereas with the second will provide us an estimate of their impact on the global distribution of LG variables. We proceed computing distribution functions for masses and velocities and show the outcomes in Table A3 and Fig. A1.

In this work we study the dynamics of the Local Group (LG) within the context of cosmological models beyond General Relativity (GR). Using observable kinematic quantities to identify candidate pairs we build up samples of simulated LG-like objects drawing from $f(R)$, symmetron, DGP and quintessence *N*-body simulations together with their ΛCDM counterparts featuring the same initial random phase realisations. The variables and intervals used to define LG-like objects are referred to as Local Group model; different models are used throughout this work and adapted to study their dynamical and kinematic properties. The aim is to determine how well the observed LG-dynamics can be reproduced within cosmological theories beyond GR, We compute kinematic properties of samples drawn from alternative theories and ΛCDM and compare them to actual observations of the LG mass, velocity and position. As a consequence of the additional pull, pairwise tangential and radial velocities are enhanced in modified gravity and coupled dark energy with respect to ΛCDM inducing significant changes to the total angular momentum and energy of the LG. For example, in models such as $f(R)$ and the symmetron this increase can be as large as 60%, peaking well outside of the 95% confidence region allowed by the data. This shows how simple considerations about the LG dynamics can lead to clear small-scale observational signatures for alternative scenarios, without the need of expensive high-resolution simulations.

From these results we conclude the following:

- The shapes of all the distribution functions are largely unaffected by both cosmic variance and resolution.
- The variance between different random realisations (both at the 256^3 and at the 512^3 level) is the largest source of differences in the parameters distribution, as can be seen in the comparison between the two 256^3 realisations (I) and (II) and also by looking at different 512^3 simulations that share the same 256^3 WN field.
- Increasing the resolution from 256^3 to 512^3 does not bias the distributions of masses, velocities and in the total number of objects-per-model found.

These results show that the conclusions drawn in the present *paper* are not affected by particle resolution, at least within the range of halo masses considered here. Cosmic variance-related effects play a larger role, however, these are factored out from our results, since the simulations have been compared on a same-seed basis.

Table A3. SimuI and SimuII results versus the two 512^3 different short-wave realisations of the same 256^3 WN fields, using priors of Model1. $v_{\rm rad}$ and $v_{\rm tan}$ are expressed in km s^{-1}.

	SimuI			SimuII		
	256^3	$512^3(a)$	$512^3(b)$	256^3	$512^3(a)$	$512^3(b)$
$v_{\rm rad}$	$-57.85^{26.32}_{-29.74}$	$-52.60^{24.36}_{-39.27}$	$-49.96^{23.01}_{-36.93}$	$-55.62^{22.85}_{-31.65}$	$-55.06^{25.62}_{-30.22}$	$-51.36^{22.69}_{-32.56}$
$v_{\rm tan}$	$45.39^{26.35}_{-17.31}$	$48.77^{28.34}_{-22.92}$	$42.04^{28.12}_{-16.59}$	$44.73^{32.14}_{-16.67}$	$45.08^{28.88}_{-21.98}$	$42.78^{30.54}_{-19.46}$
$\log_{10} M_{tot}$	$12.14^{0.14}_{-0.17}$	$12.13^{0.14}_{-0.15}$	$12.13^{0.12}_{-0.14}$	$12.15^{0.13}_{-0.16}$	$12.13^{0.13}_{-0.15}$	$12.12^{0.14}_{-0.14}$
M_{ratio}	$1.58^{0.82}_{-0.38}$	$1.63^{0.68}_{-0.37}$	$1.56^{0.74}_{-0.35}$	$1.70^{0.61}_{-0.45}$	$1.57^{0.68}_{-0.31}$	$1.62^{0.67}_{-0.38}$

Figure A1. Distribution functions for $v_{\rm rad}$, $v_{\rm tan}$ and $M_{\rm LG}$; each panel shows SimuI and SimuII (solid black lines) versus the two higher-resolution re-simulations (a) (dotted red lines) and (b) (dashed blue lines).